Proceedings of the ASME 2018 Internal Combustion Engine Fall Technical Conference
ICEF2018
November 4-7, 2018, San Diego, California, USA

ICEF2018-9627

EXPERIMENTAL INVESTIGATION OF SOOT ACCUMULATION AND REGENERATION IN A CATALYZED GASOLINE PARTICULATE FILTER UTILIZING PARTICULATE QUANTIFICATION AND GAS SPECIATION MEASUREMENTS

Dhruvang Rathod
Clemson University
Greenville, SC, USA

Dr. Simona Onori
Stanford University
Stanford, CA, USA

Dr. Zoran Filipi
Clemson University
Greenville, SC, USA

Dr. Mark Hoffman
Auburn University
Auburn, AL, USA

ABSTRACT

Recent particulate regulations for gasoline passenger cars have prompted the utilization of Gasoline Particulate Filters (GPF's) to mitigate particulate emissions. This study overviews a comprehensive experimental methodology for examination of essential GPF parameters: spatial exothermic temperature rise, particulate trapping efficiency, and the pressure rise versus particulate loading. A GDI vehicle equipped with a subfloor catalytically washcoated GPF downstream of the three-way catalyst was operated on a chassis dynamometer for data collection. Accelerated soot accumulation procedures were developed to expedite the testing while avoiding passive particulate regeneration based on both particulate concentration and size distributions. Soot concentrations pre and post GPF were used to measure the soot trapping efficiency and total soot accumulation. Fuel-cut coast events, common in real-world driving, were utilized to initiate worst case GPF regenerations, namely regenerations which produce maximum temperature rise due to the limited exhaust flow through the GPF. CO_2 measurements simultaneously measured before and after the GPF were examined to calculate the quantity of soot burned during each regeneration event. Thermocouples located inside the GPF were implemented to obtain the spatially disparate, transient temperature traces and analyzed to obtain insights on the soot distribution inside the GPF. The maximum exothermic temperature rise within the GPF was tracked for different soot loadings and regeneration temperatures to ensure GPF substrate and catalytic washcoat health. Most initial soot loadings required multiple 'fuel-cut coast' regenerations for complete soot oxidation of all trapped particulate mass.

Additionally, externally supplied oxygen was utilized to obtain complete GPF regeneration in a single event. This purpose built system created O_2 availability while maintaining constant GPF temperatures, similar to actively commanding lean A/F ratios during vehicle operation. Emissions measurements indicated that this system successfully regenerated all GPF soot. However, due to magnitude disparity between exhaust flow and total exothermic heat released, the thermocouples inside the GPF recorded only minimal exothermic temperature rises, providing confidence that lean active regeneration strategies pose little threat to GPF health.

INTRODUCTION

Gasoline Direct Injection (GDI) engines have become increasingly popular in the light duty vehicle market due to their enhanced precision fuel injection capability and thermodynamic benefits from in cylinder fuel evaporation. Thanks to these advantages, GDI engines have shown 5-15% fuel economy improvement over the conventional Port Fuel Injection (PFI) engines [1]. However, GDI engines have also found to be the source of fine and ultra-fine particulate emissions, which are detrimental to human health. Utilization of Gasoline Particulate Filters (GPF) on GDI engines, mitigates tailpipe particulate emission.

Particulate Production in GDI Engines

In-cylinder fuel injection, atomization and evaporation results in increased particulate emission formation relative to PFI engines, which depends on a myriad of parameters: engine speed, engine load, injection timing, injection targeting, ambient

conditions, etc. [2-9]. Particle emissions from a combustion engine can be divided into two categories: volatile and solid particles. The volatile, ultra-fine nanoparticles are usually formed by nucleation of sulfuric acid, water, and other species. The solid particles are termed as 'soot', which are the product of agglomerated carbon particles [10].

Chan T., et al [8] utilized a GDI engine that produced 10 and 31 times higher particulate emissions compared to PFI engine for FTP-75 and US06 cycles, respectively. Chan, T et al. [9] studied the impact of ambient temperature on particulate emissions and determined that cold ambient temperature wielded greater impact on the ultrafine particle emissions than for solid particle emissions. Their 'bag1' emissions (collected during the first 505 sec of the emissions test) from an FTP-75 cycle showed a 43% increase in solid particle number emissions from the GDI engine at ambient temperature of -18˚C compared to room temperature emissions. Once the engine was fully warm disparate ambient temperatures had no effect on the particulate emissions.

Gasoline Particulate Filters

Particulate Matter (PM) mean diameters are typically smaller from GDI engines than diesel emissions. Y. Li et. al [11] studied exhaust PM from light duty vehicles and a comparison of size particles from three different vehicles are shown in table 1. The geometric mean diameters of soot particles are smaller than those generated by diesel engines. Thus, mitigation of gasoline particulates requires tailor made GPFs rather than implementation of well-studied DPFs.

Engine Type	Test	GMD (nm) nucleation mode	GMD (nm) accumulation mode
GDI	FTP-1	11.9	45.4
	FTP-2	11.5	42.3
PFI	FTP-1	8.9	42.5
	FTP-2	8.5	35.4
Diesel	FTP-1	6.6	58.4
	FTP-2	6.5	45.9

Table 1. Geometric mean diameter (GMD) of particles from GDI, PFI and diesel engines [11].

Dairene Uy et. al [12] studied the morphology, chemistry and wear characteristics of gasoline soot and its comparison to diesel soot. It was found that soot arising from a GDI engine had more amorphous-like structure compared to diesel soot. This disorderly nanostructure makes the soot particles from gasoline engines more polar and reactive. This additional disparity in the particle characteristics further drives the need to independently research Gasoline Particulate Filters.

GPF Implementation

Equipping their GDI engine with a GPF, Chan T., et al [7] reduced the particulate emission rate down to just two and eight times higher than PFI engines for FTP-75 and USO6 drive cycles, respectively. Similar research works [13-17] have shown the effectiveness of GPF under different driving scenarios to reduce the particulate emissions in a GDI engine.

Catalytic Washcoated GPFs

Richter, J. et al. [18] and Xia, W. [19], both concluded that GPFs coated with catalytic material are preferred for soot regeneration, especially for vehicles operating in city driving conditions, where exhaust temperatures are relatively low. The authors in [18] also investigated different configurations of TWC and GPF to analyze the complete after-treatment system as a whole and found that a close-coupled TWC and GPF with an optimized catalytic coating helps further reduction of NOx emissions with no effect on fuel consumption. Washcoated GPFs were noted to increase pressure drop relative to an uncoated GPF. However no loss in fuel economy was observed during drive cycle operation [19]. It was also concluded that with an optimized precious metal coating and selective substrate, the TWC can be replaced with a coated GPF without affecting emission reduction capability.

Impact of Ash Accumulation

While the accumulated soot can be oxidized with regeneration events, either passively or actively, the byproduct of such oxidation reaction is an incombustible material, known as ash. It is important to understand the formation of ash since its accumulation will increase backpressure. Sappok et al. [20], studied the effects of ash on GPF filtration efficiency and found that even minimal ash loadings of 1 to 2 grams significantly improved the filtration efficiency of catalytic washcoated GPF by 60 to 80% with a small increase in backpressure. The amount of ash accumulated in a GPF depends on the porosity of filter substrate, soot accumulation, and temperature [21-24].

GPF Regeneration Control

Factors that affect the combustion of soot particles include exhaust gas inlet temperature, oxygen content, flow rate and accumulated mass of soot [25]. Unlike DPFs, GPFs are operated in stoichiometric conditions and at higher exhaust temperatures, stimulating the development of GPF soot regeneration control strategies. Arunachalam et al. [26] proposed a control oriented GPF model to predict the thermal dynamics during regeneration events. Van Nieuwstadt et al. [27], proposed control strategies, i) to monitor soot estimation using an empirical open loop model ii) to use spark retard to initiate regeneration and iii) for safe GPF operation controlling exothermic temperatures during regeneration using air flow.

GPF models, and subsequent control development, require detailed experimental characterization data. The experimental methodology overviewed herein results in the collection of GPF data relevant for physics-based and control oriented GPF model development. This paper is organized as follows: First, the experimental setup and instrumentation are described, followed by a description of prelimary tests, which must be conducted on a green GPF. Then, a methodology for expedient soot accumulation is overviewed. GPF regeneration studies and lessons learnt are then showcased. Finally, an external O_2 injection strategy for GPF regeneration is overviewed and the findings are related back to real world GPF operation. The paper then terminates with conclusions.

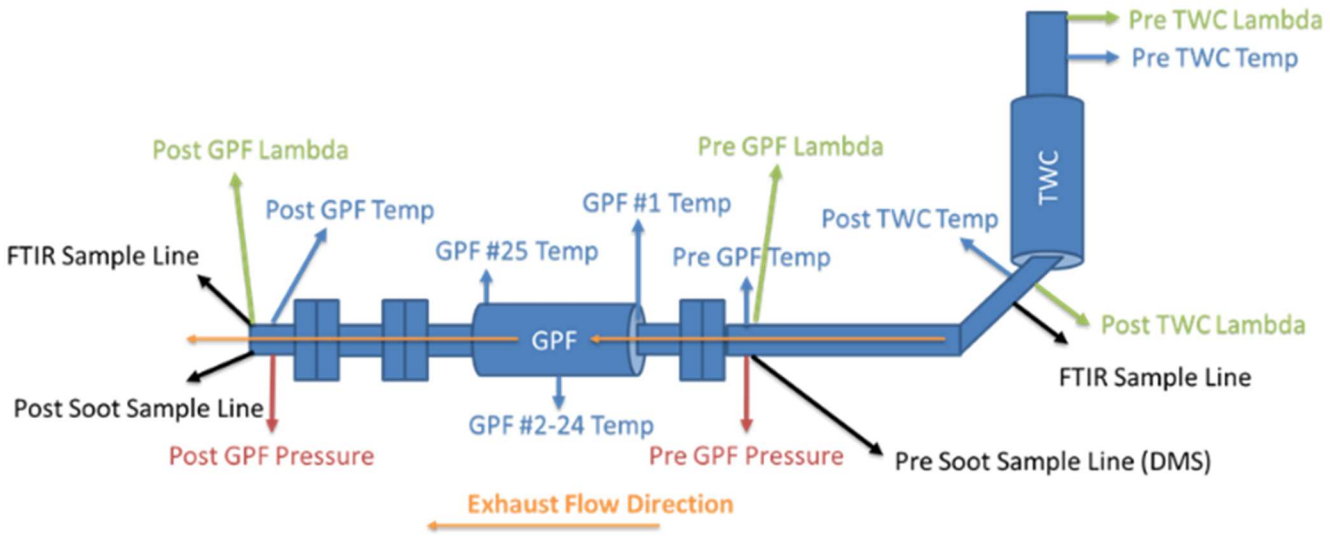

Figure 1. GPF experimental setup showing temperature, pressure, lambda sensor layout along with emission measurements.

EXPERIMENTAL SETUP AND INSTRUMENTATION

Experiments were conducted on a production vehicle with a 2.0 L, 4-cylinder, turbocharged, GDI engine via a chassis dynamometer. The stock vehicle utilized a TWC downstream of the turbocharger and a secondary TWC in a subfloor location. The subfloor TWC was removed and replaced with a GPF for this investigation. After-market tuning software was used to record data from the engine control unit, ECU. The software allowed access to spark timing and injection timing maps which were subsequently altered to facilitate expedient particulate accumulation. Manifold pressures and temperatures, engine indicated mean effective pressure, spark timing, injection timing and fuel flow were recorded with an AVL IndiSmart data acquisition system.

Figure 1 illustrates the experimental setup. Oxygen concentrations were measured using wide band air-to-fuel ratio ('lambda') sensors. Pre and post TWC lambda sensors were utilized to monitor engine operation while lambda sensors across the GPF revealed soot oxidation during regeneration. For enhanced accuracy, a dual-channel AVL i60 FTIR (Fourier-transform infrared spectroscopy) simultaneously analyzed exhaust gases before and after GPF to measure CO and CO_2 production during soot oxidation events.

In addition, a Cambustion DMS500 differential mobility spectrometer sampled upstream of the GPF to provide real time measurements of particle size distribution, number and mass at various engine operating conditions. Both particle number and mass distribution data was beneficial in identifying the operating point for aggressive soot accumulation. Additionally, photoacoustic soot quantification was provided by a single channel AVL Micro Soot Sensor, which could be switched to measure either pre or post GPF soot concentrations. Finally, pressure drop across the GPF was measured using a differential pressure transducer (*Accuracy*: 0.08% linearity, hysteresis and repeatability combined).

GPF construction and properties

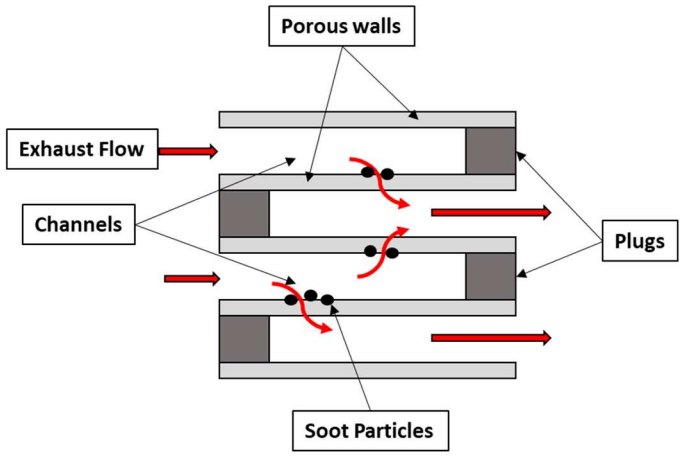

Figure 2. Pictorial representaion of GPF substrate and its functionality

The GPF consists of a cordierite substrate with channels alternatively plugged at either the inlet or the outlet. Thus, exhaust gases are forced to flow through the porous wall as shown in Figure 2. The porous wall then traps soot particles flowing with the exhaust gases. With time this trapped soot particles create additional restriction to the exhaust gas flow, increasing backpressure to the engine and impacting engine performance. To mitigate the negative backpressure impacts caused by the accumulating soot, the GPF undergoes periodic cleansing or regeneration via oxidation of the trapped soot particles.

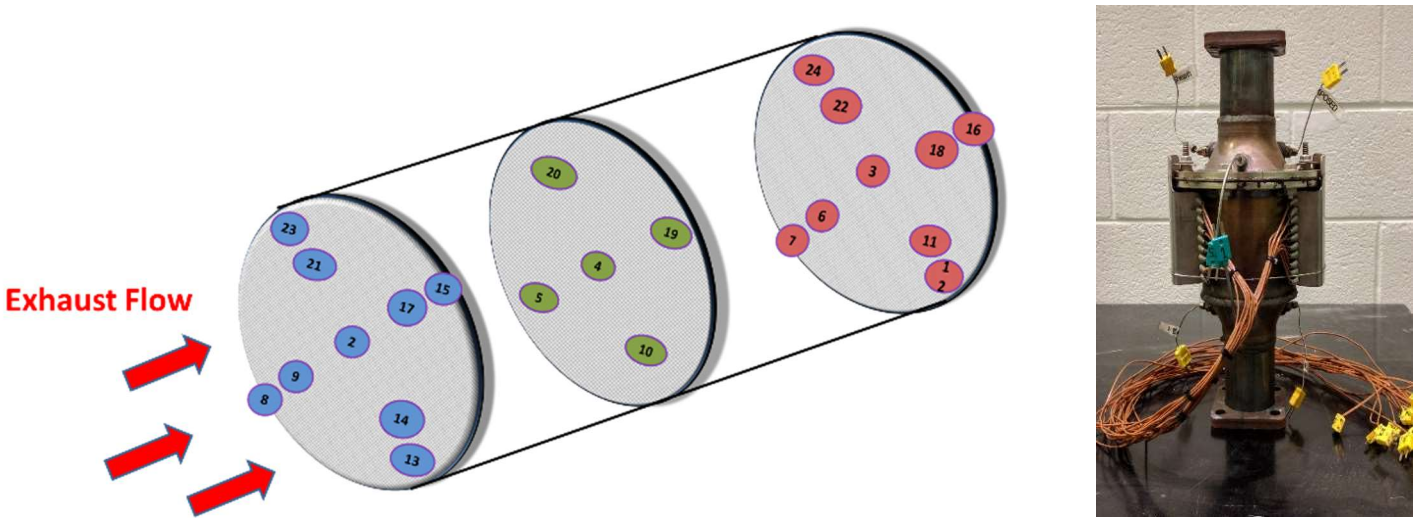

(a) (b)

Figure 3. Thermocuple layout across GPF. (a) in schematic form, and (b) on the experimental hardware

The GPF inlet and outlet exhaust gas temperatures were monitored with exposed junction J-type thermocouples located along the flow centerline in the inlet and outlet cones. Additionally, twenty four k-type thermocouples were mounted at various spatial locations within the GPF to elucidate thermal gradients during accumulation and regeneration events. The thermocouples are inserted into open GPF channels from the rear of the device. The thermocouple locations are schematically represented in Figure 3a, while a picture of the instrumented GPF device is shown in Figure 3b. Figure 3a shows three planes of thermocouples. The front plane is 1.5" inch from the front face, the mid plane thermocouples are at the center of the GPF and rear plane is at 1" from the rear face of the substrate. The front and rear plane contain pairs of thermocouples installed with a known separation distance relative to one another along a radial line. Thus, the thermocouples provide concentric rings of temperature information. These thermocouples can provide information regarding the temperature gradients experienced within the GPF and provide insights on projected device health.

Geometric parameter	value
Substrate diameter	118 [mm]
Substrate length	127 [mm]
Plug length	5 [mm]
Width of inlet channel	1.26 [mm]
Total number of channels	5085
CPSI	300 [cells/in^2]
Average porosity of the wall	0.625
Substrate volume	0.725 L
Particulate filter density	1100 [kg/m3]

Table 2. Geometric properties of the washcoated GPF.

CLEAN GPF CHARACTERIZATION

Characterization tests were conducted before accumulating any soot inside the GPF. Establishing pressure and thermal dynamic trends prior to any soot accumulation facilitates model identification of baseline GPF parameters and allows subsequent behavioral disparities to assume physical meaning.

GPF Pressure Drop Behavior

Traditional soot accumulation models correlate filter backpressure with accumulated soot mass [28, 29]. In order to utilize filter backpressure for subsequent soot mass or ash estimation, the clean filter backpressure must be characterized across an array of mass flow rates.

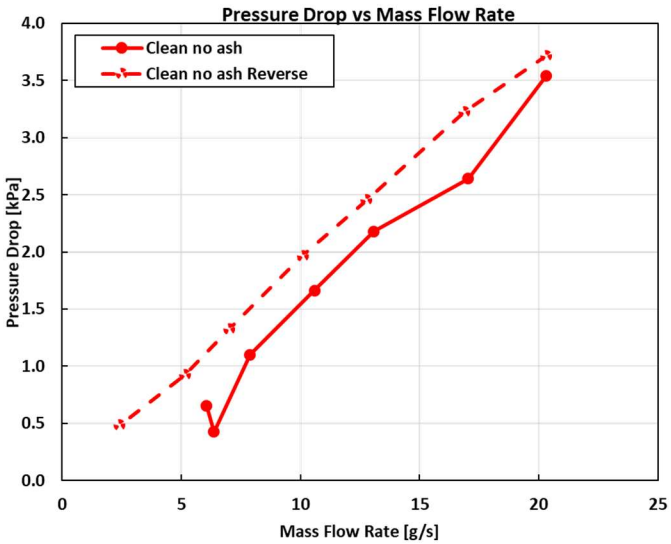

Figure 4. Plot shows pressure drop across GPF at different mass flow rates. [During the 'Reverse' testing, the operating points were run from higher flow to lower flow]

Figure 4 exhibits results from a clean filter backpressure characterization test. Note that the engine traverses from low to high mass flow rates and this procedure is reversed to check for hysteresis. The immediately subsequent 'reverse' testing exhibited higher pressure drop for identical mass flow rates, indicating that the GPF pores rapidly fill with soot particles, enhancing particle trapping during the reverse test (and increasing backpressure).

Clean GPF Temperature Dynamics

Prior to soot accumulation, the lumped thermal inertia of the cordierite and catalytic washcoat should be determined. Establishing a thermal inertia baseline for the clean GPF allows separation of exothermic heat production from baseline thermal inertia in subsequently designed GPF models. For this test, the vehicle was operated at different engine speeds using cruise control, allowing the GPF temperatures to stabilize before changing the operating point. Figure 5 below illustrates the temperature profile for GPF inlet thermocouple #1 for this test sequence.

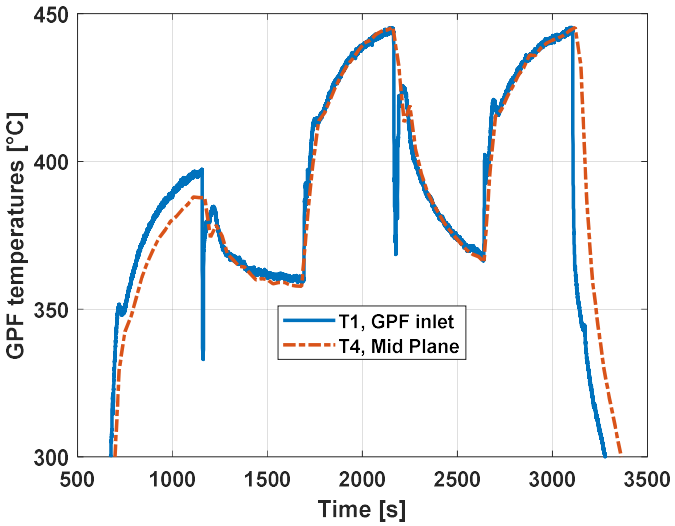

Figure 5. Temperature variation of thermocouple #1(pre-GPF)

AGGRESSIVE SOOT ACCUMULATION

Engine Operating Point Selection

The end goal of determining the internal GPF temperature behavior during soot regenerations at multiple soot concentration levels necessitates a methodology for rapidly accumulating soot in the GPF. The first step in this process is characterizing the vehicles particulate emission behavior over the operating map and establishing the sensitivity of that behavior to manipulatable factors (e.g. injection timing).

To determine an appropriate operating point for expeditious soot accumulation, particulate mass concentration were measured at different speed-load points as shown in Figure 6. The map utilized the data recorded with the Cambustion DMS 500 and span the relevant operational range for drive cycles. Although high particulate concentration is important for rapid soot accumulation, if the GPF experiences significant particulate breakthrough during the operation (inefficient particulate trapping), the raw particle count may become an important consideration in selection of the engine operating point. In general, large soot particles will fill up the porous wall of the GPF and will in turn act has additional blockage to the incoming soot particles, resulting in higher trapping efficiency.

The mass of soot entering the GPF can be calculated by using the Microsoot soot concentration measurement (in mg/m^3) and the exhaust flow. To ensure accuracy in the calculated soot mass, the engine must be operated at a constant speed and load point to achieve constant mass flow.

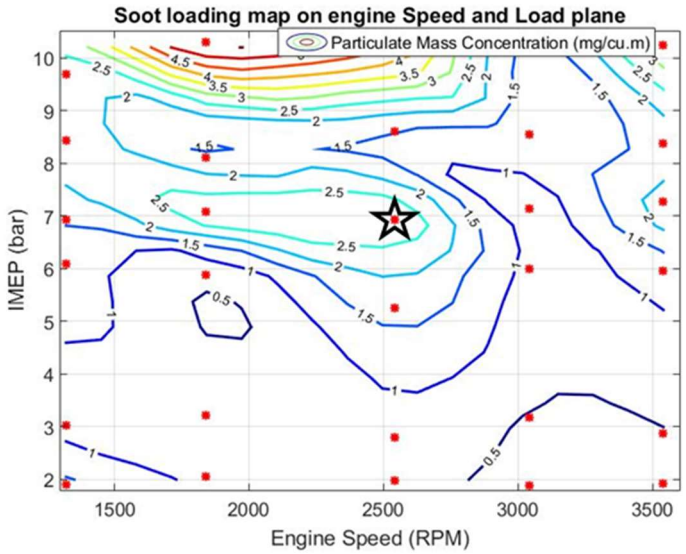

Figure 6. Contour plot of Particulate Mass at different engine speed and load points (red points are the measurements).

It was observed from figure 6 that operating above 9 bar or above 3200 rpm produced the largest soot particles and highest mass concentrations. However, operating at such high load points resulted in instrumentation error because of vibration inside DMS. From figure 6, it was noted that 2540 rpm and 7 bar (highlighted with a star) will be a good starting point towards evaluating the possible accumulation point.

Impact of Injection Timing on Particulate Production

During experimentation, particulate production exhibited the strongest sensitivity to injection timing. Therefore, injection timing is presented herein as the key actuator enabling expedient GPF soot accumulation. At the operational point selected for maximum soot production, 2540 rpm 7 bar, an injection sweep was also performed to establish the sensitivity of soot production to injection timing. As seen from Figure 7, a 40 CAD advanced injection timing produced the largest quantity of soot particles.

This was attributed to cylinder wall and piston surface fuel impingement resulting in wall wetting and possibly fuel pooling. These rich zones then serve as the ideal source for soot generation.

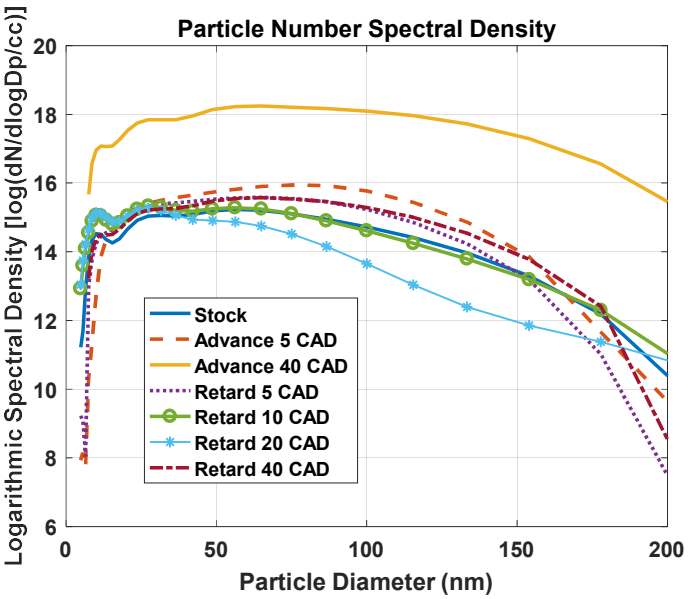

Figure 7. Particle Size and density variation with respect to injection timing

Effects of Exhaust Temperature

With intermittent lambda excursions during normal engine operation, passive soot oxidation can occur in the catalytically washcoated GPF at inlet temperatures greater than 500°C [30]. The final criteria in selection of engine operating point for the soot accumulation test was based on this 500°C exhaust temperature constraint. Maintaining exhaust temperatures below 500°C during accumulation ensures that all particulates generated by the engine accumulate inside GPF, and validates the accuracy of the soot mass accumulation calculations.

A map of engine exhaust temperature versus operating condition was experimentally determined, see Figure 8. This data, in combination with the particulate production mapping shown in Figure 7, resulted in the selection of 1360 RPM and 6bar IMEP with 40 CAD advanced injection timing as the most advantageous operating point for enhanced soot accumulation.

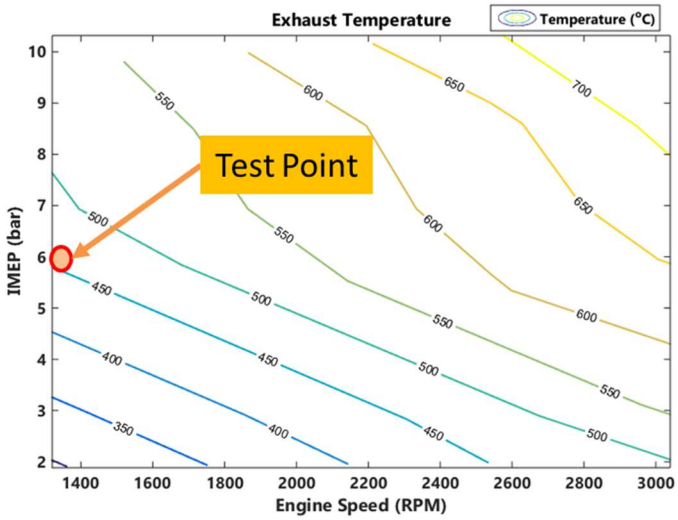

Figure 8. Exhaust temperature map at different engine speed and load points.

SOOT ACCUMULATION TESTING

The vehicle was maintained at the identified speed and load operating point [1360 rpm and 6 bar with 40 CAD advanced injection timing] using cruise control. GPF inlet and outlet soot concentrations were then measured to determine trapped soot mass. Since the microsoot was a single channel analyzer, inlet and outlet measurements were taken sequentially while maintaining steady engine operation. Two minute recordings for pre GPF and post GPF locations were averaged to establish a time varying trapping efficiency, which was in turn utilized for soot accumulation calculation. Figure 9 shows typical analyzed accumulation data.

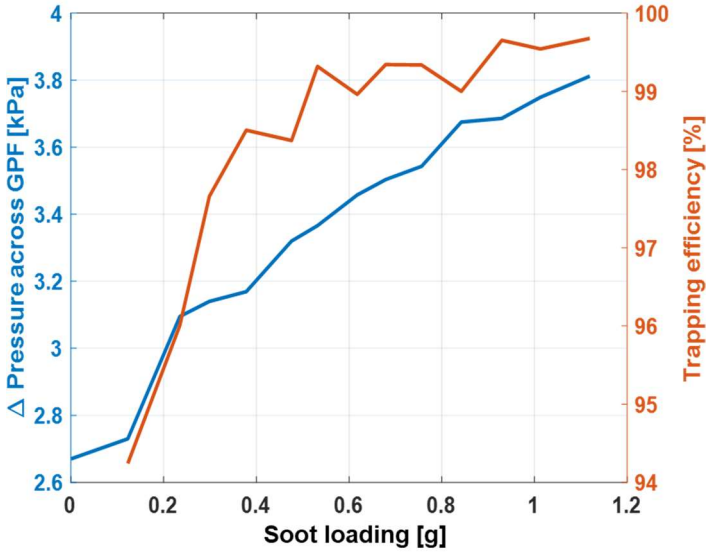

Figure 9. Pressure drop across GPF and mass based trapping efficiency trends with respect to soot loading during an accumulation test.

For the non-green GPF illustrated in Figure 9, a pressure drop of 2.67 kPa at 0 g of soot loading is the result of both

exhaust flow restriction and ash accumulation. As the soot accumulates at the constant engine speed, the component of pressure drop due to the exhaust flow remains constant. During accumulation tests, the exhaust temperatures are below the passive regeneration trigger point, and therefore the pressure drop due to ash accumulation is also constant. Thus, any increment in pressure drop during the soot accumulation test is due to soot accumulation only. Additionally, blockage of wall pores with accumulating soot creates additional restriction to the exhaust flow and increases the GPF trapping efficiency during accumulation.

Figure 10 illustrates the soot accumulation testing from a cold start to the desired soot level. As engine runtime increases, the coolant temperature also increases, reducing soot production. To better correlate this phenomenon, the soot concentration measurement was recorded non-stop at the preGPF location.

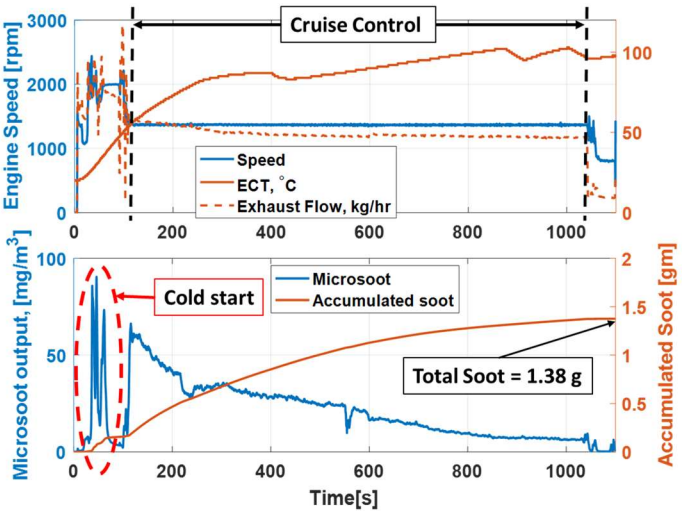

Figure 10. Engine speed, coolant temperature and exhaust flow rate during an accumulation test (top), and the soot loading profile during accumulation test (bottom).

The soot loading profile, see Figure 10 (bottom plot), shows that the maximum rates of soot production occurred at cold start, as expected. Soot production then continually drops while the operating conditions are held constant due to the increasing engine coolant temperature (ECT). As the ECT cycles near its control temperature of 100˚C, soot production rate stabilizes at its lowest value. Applying equation (1), total soot accumulation was calculated to be 1.38 g or 0.8 g/L using an average trapping efficiency of 98%. Therefore, the most expedient time-based soot accumulation is attained by initiating each accumulation test from a cold start. A two hour forced cool down between tests adequately reduces the coolant temperature to ~23˚C.

Equation for Soot Loading Density (SLD):

$$\text{SLD} = \frac{\varepsilon_T \int \text{SLR}\, dt}{V_{GPF}} \qquad (1)$$

SLR = Soot Loading Rate [g/s]
V_{GPF} = GPF Volume, L
ε_T = Trapping Efficiency

REGENERATION TESTING

Engine backpressure rises proportionally to the quantity of soot accumulated in the GPF, hindering engine breathing and affecting the volumetric efficiency. To prevent negative impacts on engine fuel economy, the accumulated soot must be periodically removed from the GPF through oxidation. The initiation and completion of this oxidation process is termed as GPF *Regeneration*.

Elevated temperatures and oxygen must both be present to trigger soot oxidation. In a gasoline vehicle setup, temperatures compatible with soot oxidation can be achieved by increasing the engine load and/or retarding the ignition timing. However, excess oxygen is only available at a post TWC location through intentional leaning of the air fuel ratio or during fuel cut coast-down conditions that occur during real-world driving. Therefore, in this work, the engine is first ramped to a high load operating point until the desired exhaust temperature is attained and then the regeneration event is initiated by a throttle tip-out, which results in a fuel-cut coast of the vehicle on the chassis dyno.

Multiple regenerations were performed at different tip-out temperatures with various soot loadings. In general, exothermic temperature rise was highly tied with tip-out temperature. To maintain safe operation and GPF health, the GPF supplier specified a recommended maximum internal GPF temperature of 900°C. *Note that*: Due to limited ECU control authority, there was no means to alter engine operation to force lean excursions while simultaneously maintaining high exhaust temperatures. Hence, tipouts were the only means to attempt soot oxidation.

Test Conditions

Figure 11, shows the engine conditions and GPF temperature traces during a representative fuel-cut tip-out regeneration event. Vehicle fueling and resultant pre and post GPF lambda signals are also provided in Figure 12.

After throttle tipout, the engine fueling stops (Figure 12, bottom plot) and both the engine and vehicle speeds decrease rapidly (Figure 11, top). Once fuel injection has ceased, the engine functions as an air pump for the coast down period, supplying the oxygen necessary for the post TWC GPF to regenerate, but also decreasing the GPF inlet temperature, bottom plot of Figure 11, and limiting the time frame in which GPF temperatures are elevated enough for oxidation.

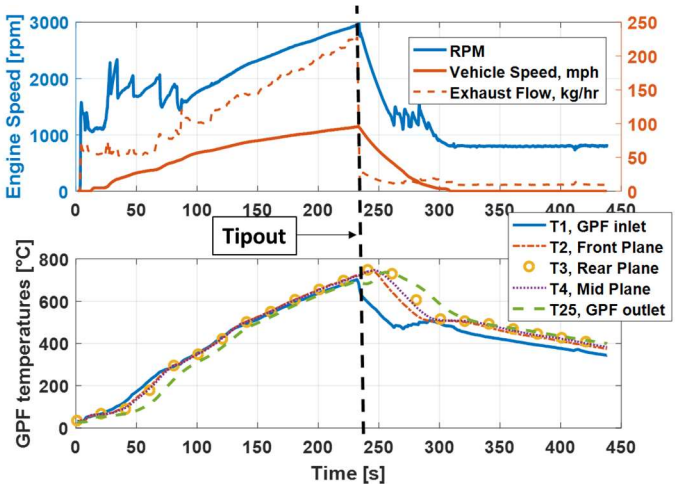

Figure 11. Engine conditions during regeneration testing (top) and GPF temperature variation during a regeneration test at 700˚C (bottom)

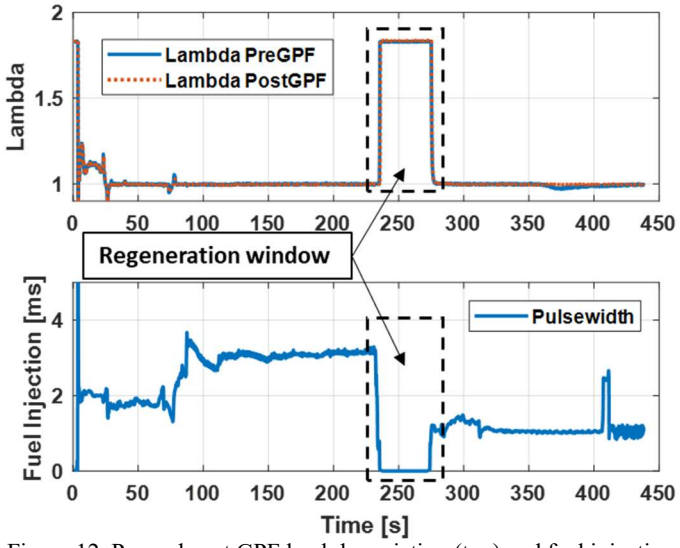

Figure 12. Pre and post GPF lambda variation (top) and fuel injection pulse width (bottom) during a regeneration test at 700˚C. The fuel cut-off lasted for 38 sec.

Regeneration Analysis

The resulting GPF temperature traces along the axial centerline are shown in Figure 13. Nearly all regeneration tests exhibited their maximum temperature rise at the rear most measurement location plane, which logically agrees with expected spatial distribution of soot accumulation

In order to eliminate the difference of initial tip-out temperature for all 25 sensors, data is analyzed with respect to Delta Temperatures. Figure 14 shows such a plot of delta temperatures. Equation 2 is used to calculate the delta temperature at each sensor location.

$$\Delta T_n = \max(T_n) - T_{n,tipout} \quad (2)$$

Where n indicates the n[th] sensor and ΔT_n= represents the temperature rise with respect to tip-out temperature for that given thermocouple

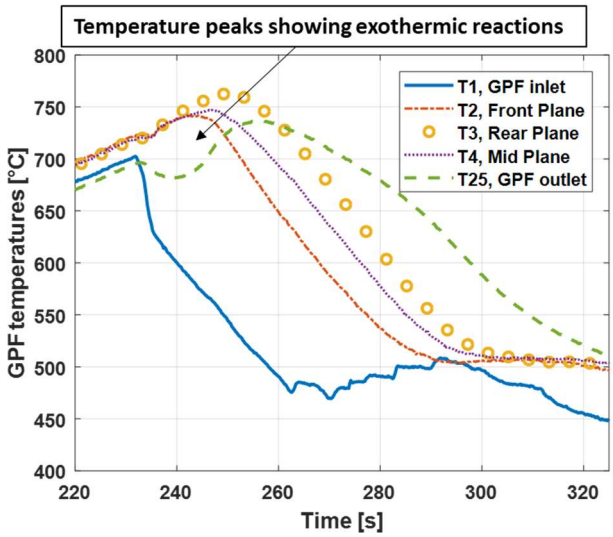

Figure 13. Temperature variation at three different GPF locations compared to inlet and outlet GPF temperatures

Figure 14 illustrates the temperature rise of each internal GPF temperature relative to its own temperature at the time of tip-out. In this fashion, the relative intensity of the spatially disparate exotherms can be compared throughout the GPF.

As seen from the Figure 14, the highest temperature rise is seen by the rear plane thermocouple (#3) followed by the exit location #25. Thermocouple #25 is located outside the substrate along the exhaust flow centerline. The temperature rise seen at #25 (Figure 13) is created superimposing multiple effects. Namely, after throttle tipout the engine speed decreases, reducing the exhaust mass flow and slowing the transport of exothermic heat generated inside the GPF during regeneration. Hence, a phase shift in temperature rise is observed in the GPF exit temperature (location #25) in Figure 13.

Note that the rear plane peripheral thermocouple locations 7, 12, 16, and 24 do not experience exothermic temperature rise. However, adjacent thermocouples to these periphery locations (6, 11, 18, and 22), which are 8 mm radially inward, experience exothermic activity. This behavior results from two logical conditions: (i) the exterior GPF locations are more apt to lose heat to the environment, limiting their ability to oxidize soot, and (ii) soot accumulation is proportional to the total flow, which is theoretically maximized at the flow center line.

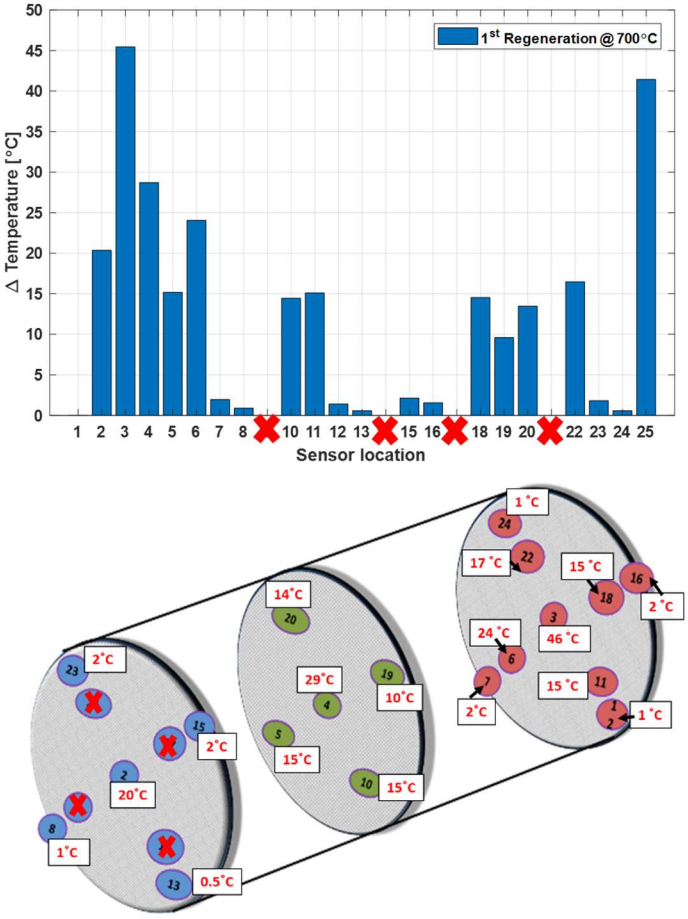

Figure 14 (a) and (b). Delta temperature rise for each internal GPF thermocouple. The crossed out thermocouples (9, 14, 17, and 21) were unresponsive due to damage suffered during installation.

Emissions Speciation Results

During regeneration, a dual channel FTIR simultaneously measured CO and CO_2 concentrations at the GPF inlet and outlet. The top and bottom plot of Figure 16 show pre and post GPF CO_2 and CO measurements, respectively. Elevated post GPF CO_2 measurements indicates oxidation of trapped carbon particles. Integration of these quantitative CO_2 results can determine the amount of soot oxidized during the fuel cut tip-out as shown by Arunachalam et.al [20].

Post GPF CO concentrations, shown in the bottom plot of Figure 15, were lower in magnitude than the pre GPF values, indicating that the oxidizing carbon particles were completely oxidizing the CO_2. Additionally, the CO concentrations were orders of magnitude lower than the CO_2 measurements, providing justification for reaction scheme simplifications during regeneration modeling Arunachalam et.al [20].

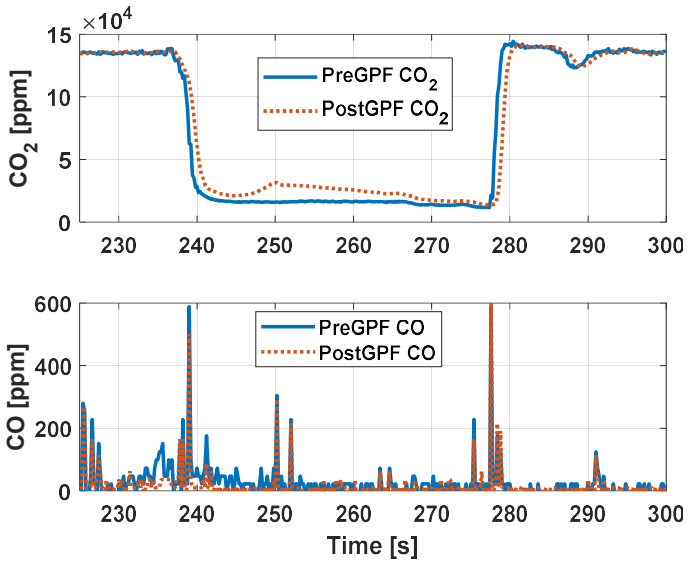

Figure 15. CO and CO_2 plots during a regeneration test

Subsequent Regeneration Tip-outs

As seen in Figure 13, the GPF inlet temperature dropped 200˚C within 26 seconds due to the throttle tipout. However, the pre and post GPF lambda signals, shown in Figure 12, indicate that O_2 availability lasted 38 seconds. The rapid GPF inlet temperature decrease limits the available time for carbon oxidation during regeneration. To ensure complete oxidation of the trapped soot particles prior to further accumulation/regeneration testing, the main regeneration was followed by subsequent tip-out events while monitoring for additional exothermic activity via the installed thermocouples.

The GPF temperature results of subsequent tipouts are compared with main regeneration event in Figure 16. The first regeneration event, with throttle tipout at 700˚C, experienced the highest GPF temperature rise. However the second tipout at the same temperature of 700˚C achieved only a 17˚C maximum temperature rise due to the reduced carbon loading. Thus, the subsequent 3rd tipout was performed at 775˚C to stimulate additional oxidation. At this elevated temperature, new locations located toward the periphery (5, 6, 10, 11, 18, 20, and 22) now exhibited the largest exothermic temperature rise. The increased inlet temperature initiates soot oxidation in locations further from the flow centerline, which are cooler due to GPF heat loss and have lower soot density. Meanwhile, there was limited soot remaining along the GPF flow centerline due to the previous tip-outs.

Additionally, the elevated inlet temperature at tipout also creates a longer duration of inlet temperatures above the 500˚C oxidation threshold, prolonging the regeneration event. Table 3 shows the time taken by the inlet temperature to drop below 500˚C and the time span of O_2 availability (fuel cut event). Subsequent tipouts were terminated after iteration 4 at 800°C,

which produces only minimal internal GPF temperature rises despite benefiting from a very aggressive exhaust temperature and the longest overlapping availability of temperature and oxygen. It was concluded at that point that no more soot remains in the GPF.

	Time	
Tip-out temperature	**O_2 availability**	**Inlet temperature > 500 ˚C**
˚C	**sec**	**sec**
700	38.6	26.2
775	43	90.8
800	41.2	111.8

Table 3. Comparison of O_2 availability duration and longevity of GPF inlet temperature (to be >500 ˚C) during different tipout events.

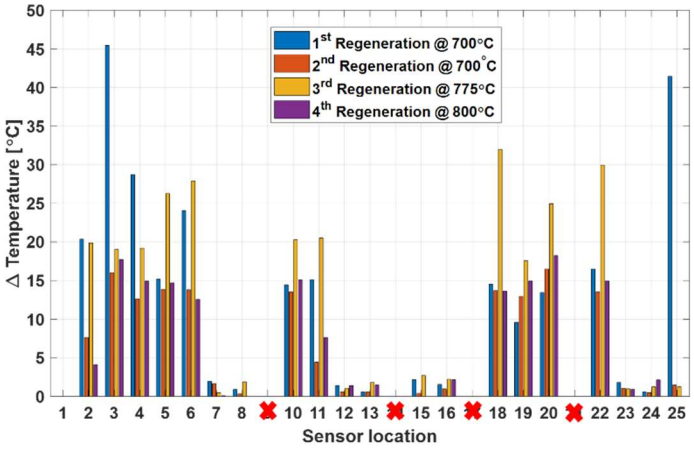

Figure 16. Temperature rise for each subsequent tipouts at higher temperatures are compared with the 1st regeneration event.

O_2 INJECTION STRATEGY

Fuel cut tip-outs produce incomplete GPF regeneration due to the rapid decrease of exhaust temperature. In order to obtain regeneration in a single event, both elevated temperature and oxygen must persist until all soot is oxidized. Since ECU control authority was limited on this setup, an external oxygen supply configured to assist the regeneration process.

Experimental Setup

Figure 17 shows the modified experimental setup required for the external supply of oxygen. Figure 18 shows the diffuser manufactured and installed at the end of one way check valve for even distribution of the oxygen into the exhaust stream.

Additional components were required needed for successful implementation of external supplied oxygen:

1. *A Pressure Regulator* was utilized to reduce the O_2 tank pressure, and aided the upstream pressure control for proper functioning of the mass flow controller.
2. A mass flow controller accurately metered the oxygen flow into the exhaust stream. Specifically, a Teledyne Hastings Instruments Controller was installed with 0-500 SLM Full scale range. Accuracy ± (0.5% of reading + 0.2% of full scale). Repeatability ± 0.15% of full scale.
3. *Heated lines* were utilized to avoid reduction of exhaust temperature after O_2 mixing, heated lines increased the temperature of the Oxygen flow after expansion from the O_2 tank. The temperature controller for the heated lines was set to 300˚C.

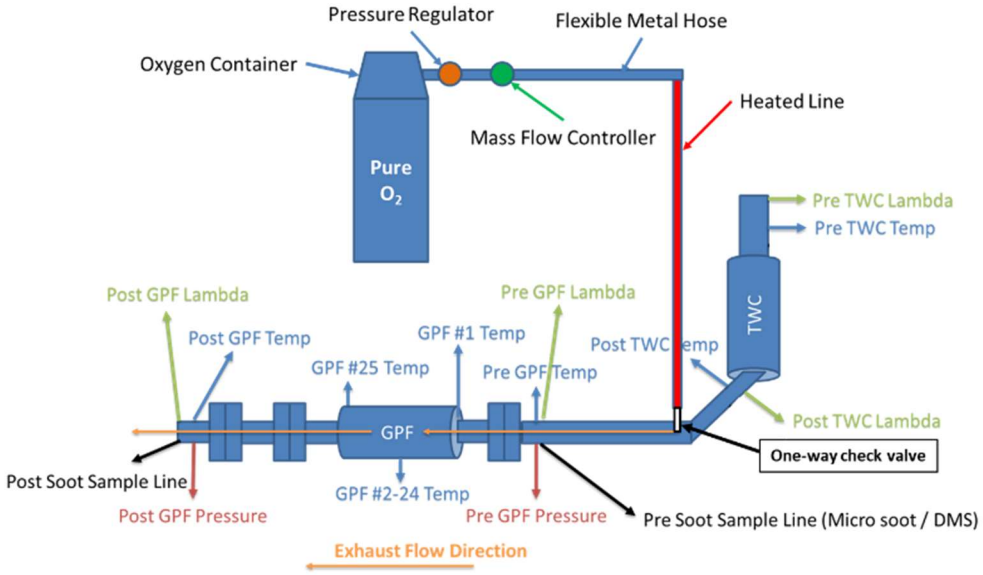

Figure 17
GPF experimental setup with external Oxygen supply

Figure 18
Designed diffuser to disperse O_2 into the exhaust stream

Regeneration via O_2 Injection - Results

This experiment was conducted in three steps. First the exhaust temperature was held at 650°C via cruise control where the recorded exhaust flow rate was 35 g/s. Oxygen was then injected to induce regeneration. Subsequently, exhaust temperature was raised to 700°C where the exhaust flow was 41 g/s to incite additional regeneration during oxygen injection. Finally, a fuel cut tipout was conducted to determine the effectiveness of the regeneration procedure.

Maximum O_2 flow was device limited to 200 LPM or 4 g/s. Therefore with an O_2 flow of 200 LPM at 35 g/s exhaust flow, the mixed exhaust gases reaching the GPF were 11.4% lean. During the second portion of the test, where the exhaust flow was 41 g/s, the 200 LPM of oxygen flow produced an exhaust gas mixture that is 9.75% lean.

Engine conditions for the O_2 injection regeneration testing are shown in Figure 19. The pressure regulator valve was manually controlled to provide the desired flow rate. Thus a gradual ramp can be seen in the bottom plot of Figure 19. Region A corresponds to the 650˚C exhaust temperature region while Region B is the 700˚C exhaust temperature region. Finally, region C was the deliberate fuel cut event without external O_2 supply. Each of this regions are analyzed individually below.

At 300 sec, O_2 flow is initiated and T1 experiences a small drop because of the cold O_2 flow, see Figure 20(top). Meanwhile, internal GPF sensors at locations 2 and 4 experience a slight temperature rise before stabilizing for the remainder of Region A. This small temperature rise represents soot oxidation, which is confirmed from the pre and post GPF CO_2 plots in Figure 20 (bottom). The Post GPF CO_2 level is consistently greater than the pre GPF measurement, indicating soot oxidation.

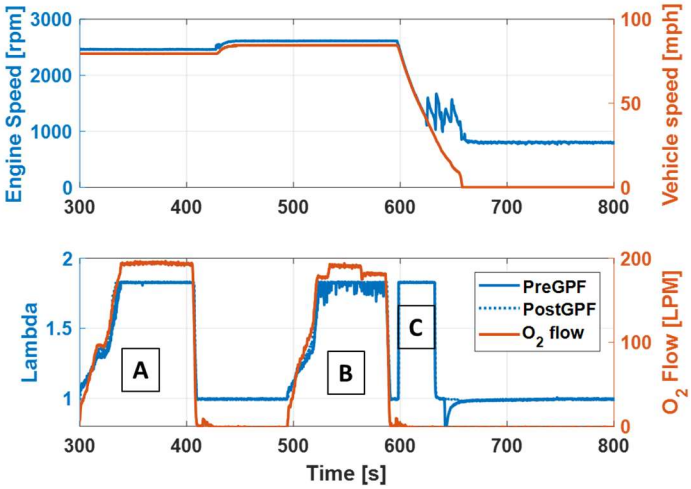

Figure 219. Engine conditions during the external O_2 supply test (top plot) and lambda variation pre and post GPF when O_2 supply was initiated (bottom plot).

Step 1 - Region A – $T_{exhaust}$ = 650 ˚C

Although soot oxidation is occurring throughout the supply of external O_2, dramatic internal GPF temperature exotherms are not observed. The exothermic temperature rise experienced during tip-out fuel cuts, as seen in Figure 11, occurs as the exhaust flow is dropping to idle flow, which is in the range of 3~4 g/s. The total exhaust gas flowing through the GPF during the O_2 injection regeneration was 39 g/s, a tenfold increase. Thus, no temperature rise was observed by the GPF thermocouples because the high exhaust flow purged away the exothermic heat very quickly.

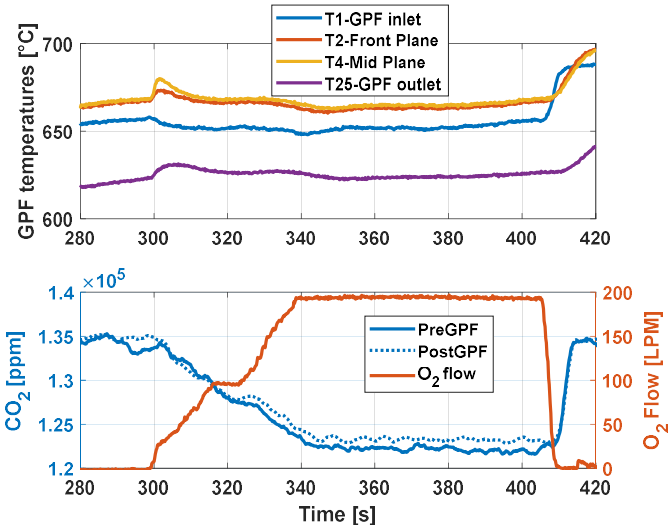

Figure 20. Region A analysis of CO_2 plots and temperature rise with external O_2 flow.

Step 2 - Region B – $T_{exhaust}$ = 700 ˚C

Region B exhibits similar behavior to Region A. As O_2 flow commences, a small upswing is seen in internal GPF thermocouples 2 and 4 but no substantial temperature rise is experienced by these thermocouples. However like region A, post GPF locations record higher CO_2 compared to the pre GPF location indicating soot oxidation.

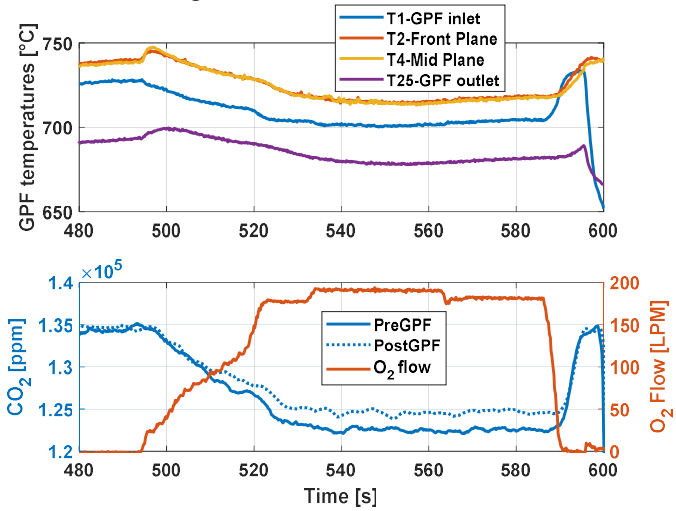

Figure 21. Region B analysis of CO_2 plots and temperature rise with external O_2 flow.

Step 3 - Region C - Fuel cut Tipout @ $T_{exhaust}$= 700 ˚C

Finally a fuel cut tipout was initiated to check for generation of any internal GPF temperature rise. No substantial temperature rise was observed at the flow centerline locations (Figure 22) or other locations inside the GPF (Figure 23). For clarity, Figure 23 is plotted with the same scale of post tip-out temperature rise as earlier results. Note that many of the internal GPF thermocouples were damaged during multiple high temperature high flow regeneration process at this point.

Post GPF CO_2 measurements are nearly identical to the pre GPF values for this tip-out, see Figure 22 (bottom), indicating that no appreciable trapped particulates remained during this tipout.

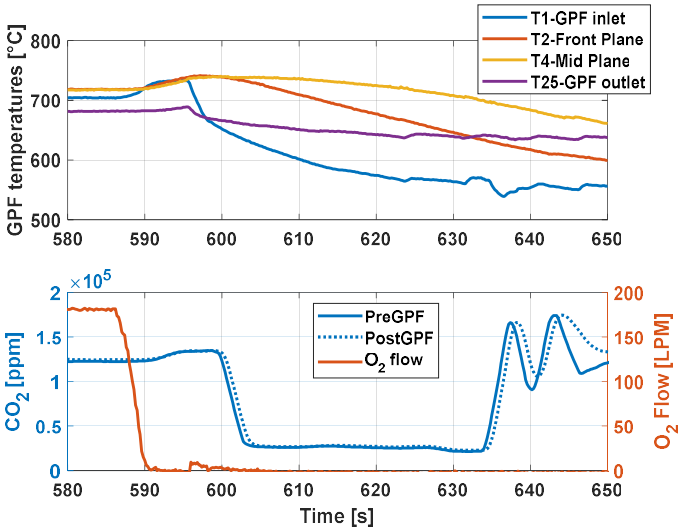

Figure 22. Region C analysis of CO_2 plots and temperature rise during a fuel cut event following O_2 injection tests

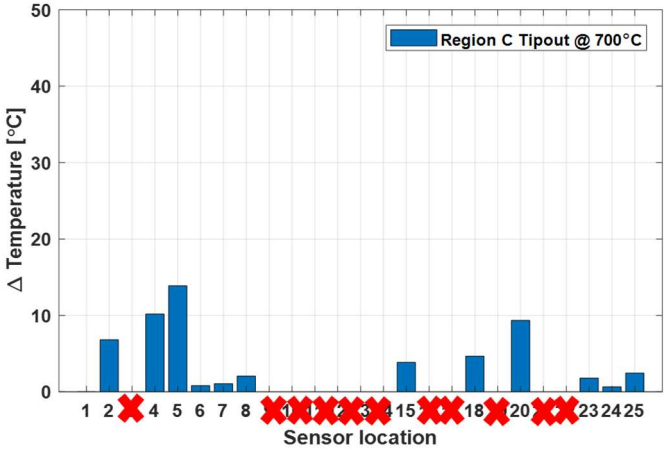

Figure 23. Region C analysis of temperature rise for each GPF locations during a fuel cut event following O_2 injection tests

CONCLUSION

This work overviews a comprehensive experimental methodology to examine vital gasoline particular filter parameters required for soot accumulation and regeneration studies and GPF modeling. An operational point suitable for rapid particulate accumulation was evaluated based on particulate density and particulate number trends across the operational spectrum along with an exhaust temperature ceiling of 500 ˚C. In addition, advancing the injection timing by 40 CAD resulted in a tenfold increase to particulate number at the chosen operational point.

Tracking GPF pressure drop during soot accumulation testing allowed separation of soot derived pressure drop from the exhaust flow pressure drop. Once characterized, this pressure drop data can track soot accumulation inside GPF during real-world driving. The GPF's trapping efficiency increased with soot loading as the porous wall in the substrate filled with soot particles.

Regeneration studies showed that spatial variations in soot accumulation are mainly a function of local exhaust flow velocity variation. The most aggressive exothermic temperature rises were observed towards the rear of the GPF, indicating that soot deposition increases as the exhaust gases slow down traversing through GPF. Additionally, most of the exothermic activity was concentrated near the center of GPF, which is simultaneously the centerline of the exhaust flow and the furthest location from external heat losses.

The rapid decrease of exhaust temperature upstream of the GPF due to a throttle tip-out limited the effectiveness of the regeneration events. Subsequent tipouts also exhibited exothermic temperature rise and increased post GPF CO_2 relative to the inlet, indicating that one fuel-cut coast event was not enough for complete GPF soot oxidation. This behavior provides confidence that real-world passive soot regeneration during fuel-cut tip-outs can mitigate GPF soot accumulation, but will create a drive-cycle dependent equilibrium soot loading within the GPF.

To achieve complete soot oxidation in one single event a scenario should be developed were both high temperature and excess oxygen is available in the exhaust stream. A dedicated oxygen injection system was constructed to enable GPF regeneration at constant exhaust temperature. While pre and post CO_2 measurements indicated regeneration activity, the high exhaust flow rate prevented large temperature swings within the GPF, i.e. the heat was transported out of the GPF very quickly. Subsequent tipout testing exhibited minimal GPF temperature rise, confirming the trapped soot was burned during the steady state O_2 injection tests without temperature swings. With higher exhaust flow, no GPF temperature runaway will be experienced. Thus, operating slightly lean or injecting air post TWC can provide a safe regeneration pathway without affecting the GPF health.

Overall, this work outlines the necessary experimental testing for characterization of a washcoated GPF and subsequent

development of: GPF thermal models, backpressure versus soot accumulation models, and multidimensional, physics-based soot regeneration models [26].

NOMENCLATURE

GPF = Gasoline Particulate Filter
GDI = Gasoline Direct Injection
DPF = Diesel Particulate Filter
FTIR = Fourier-transform infrared spectroscopy
CAD = Crank Angle Degree
ECT = Engine Coolant Temperature
LPM = Liter per minute
TWC=Three-Way Catalyst
FTIR = Fourier Transform InfraRed

Terminology
Exotherms = Exothermic reaction
Tipout = foot off the throttle event

ACKNOWLEDGMENTS

The author's gratefully acknowledge the support of Fiat Chrysler Automobiles (FCA) US LLC for technical and financial support during this study.

Dr. Simona Onori acknowledges the support of the National Science Foundation through the grant CAREER #1839050

REFERENCES

1. Brehob, Diana D., Jonathan E. Fleming, Mohammad Haghgooie, and Robert A. Stein. *Stratified-charge engine fuel economy and emission characteristics*. No. 982704. SAE Technical Paper, 1998.
2. Peckham, Mark S., Alex Finch, Bruce Campbell, Phil Price, and Marcus Timothy Davies. *Study of particle number emissions from a turbocharged gasoline direct injection (GDI) engine including data from a fast-response particle size spectrometer*. No. 2011-01-1224. SAE Technical Paper, 2011.
3. Williams, Ben, Paul Ewart, Xiaowei Wang, Richard Stone, Hongrui Ma, Harold Walmsley, Roger Cracknell et al. "Quantitative planar laser-induced fluorescence imaging of multi-component fuel/air mixing in a firing gasoline-direct-injection engine: effects of residual exhaust gas on quantitative PLIF." *Combustion and Flame* 157, no. 10 (2010): 1866-1878.
4. Velji, Amin, Kitae Yeom, Uwe Wagner, Ulrich Spicher, Martin Roßbach, Rainer Suntz, and Henning Bockhorn. *Investigations of the formation and oxidation of soot inside a direct injection spark ignition engine using advanced laser-techniques*. No. 2010-01-0352. SAE Technical Paper, 2010.
5. Lucchini, Tommaso, Gianluca D'Errico, Angelo Onorati, Giovanni Bonandrini, Luca Venturoli, and Rita Di Gioia. "Development and application of a computational fluid dynamics methodology to predict fuel–air mixing and sources of soot formation in gasoline direct injection engines." *International Journal of Engine Research* 15, no. 5 (2014): 581-596.
6. Maricq, M. Matti, Diane H. Podsiadlik, Diana D. Brehob, and Mohammad Haghgooie. *Particulate emissions from a direct-injection spark-ignition (DISI) engine*. No. 1999-01-1530. SAE Technical Paper, 1999.
7. Bonatesta, F., E. Chiappetta, and A. La Rocca. "Part-load particulate matter from a GDI engine and the connection with combustion characteristics." *Applied Energy* 124 (2014): 366-376.
8. Chan, Tak W., Eric Meloche, Joseph Kubsh, Deborah Rosenblatt, Rasto Brezny, and Greg Rideout. "Evaluation of a gasoline particulate filter to reduce particle emissions from a gasoline direct injection vehicle." *SAE International Journal of Fuels and Lubricants* 5, no. 2012-01-1727 (2012): 1277-1290.
9. Chan, Tak W., Eric Meloche, Joseph Kubsh, Rasto Brezny, Deborah Rosenblatt, and Greg Rideout. "Impact of ambient temperature on gaseous and particle emissions from a direct injection gasoline vehicle and its implications on particle filtration." *SAE International Journal of Fuels and Lubricants* 6, no. 2013-01-0527 (2013): 350-371.
10. Mathis, Urs, Martin Mohr, and Anna-Maria Forss. "Comprehensive particle characterization of modern gasoline and diesel passenger cars at low ambient temperatures." *Atmospheric Environment* 39, no. 1 (2005): 107-117.
11. Li, Y., Xue, J., Johnson, K., Durbin, T., Villela, M., Pham, L., Hosseini, S., Zheng, Z., Short, D., Karavalakis, G. and Asa-Awuku, A., 2014. *Determination of suspended exhaust PM mass for light-duty vehicles* (No. 2014-01-1594). SAE Technical Paper.
12. Uy, Dairene, Monica A. Ford, Douglas T. Jayne, Larry P. Haack, Jon Hangas, Mark J. Jagner, Alex Sammut, and Arup K. Gangopadhyay. "Characterization of gasoline soot and comparison to diesel soot: morphology, chemistry, and wear." *Tribology International* 80 (2014): 198-209.
13. Shimoda, Takehide, Yoshitaka Ito, Chika Saito, Takahiko Nakatani, Yukinari Shibagaki, Kazuya Yuuki, Hirofumi Sakamoto et al. *Potential of a low pressure drop filter concept for direct injection gasoline engines to reduce particulate number emission*. No. 2012-01-1241. SAE Technical Paper, 2012.
14. Kern, Bernhard, Stephanie Spiess, and Joerg Michael Richter. *Comprehensive Gasoline Exhaust Gas Aftertreatment, an Effective Measure to Minimize the Contribution of Modern Direct Injection Engines to Fine Dust and Soot Emissions?*. No. 2014-01-1513. SAE Technical Paper, 2014.
15. Demuynck, Joachim, Cecile Favre, Dirk Bosteels, Heather Hamje, and Jon Andersson. *Real-World Emissions Measurements of a Gasoline Direct Injection Vehicle without and with a Gasoline Particulate Filter*. No. 2017-01-0985. SAE Technical Paper, 2017.
16. Czerwinski, Jan, Pierre Comte, Norbert Heeb, Andreas Mayer, and Volker Hensel. *Nanoparticle Emissions of DI Gasoline Cars with/without GPF*. No. 2017-01-1004. SAE Technical Paper, 2017.
17. Ogata, Takayuki, Mikio Makino, Takashi Aoki, Takehide Shimoda, Kyohei Kato, Takahiko Nakatani, Koji Nagata, Claus Dieter Vogt, Yoshitaka Ito, and Dominic Thier. *Particle Number Emission Reduction for GDI Engines with Gasoline Particulate Filters*. No. 2017-01-2378. SAE Technical Paper, 2017.
18. Richter, Joerg Michael, Raoul Klingmann, Stephanie Spiess, and Ka-Fai Wong. "Application of catalyzed gasoline particulate filters to GDI vehicles." *SAE International Journal of Engines* 5, no. 2012-01-1244 (2012): 1361-1370.
19. Xia, Wenzheng, Yi Zheng, Xiaokun He, Dongxia Yang, Huifang Shao, Joesph Remias, Joseph Roos, and Yinhui Wang. *Catalyzed Gasoline Particulate Filter (GPF) Performance: Effect of Driving Cycle, Fuel, Catalyst Coating*. No. 2017-01-2366. SAE Technical Paper, 2017.

20. Sappok, Alexander, Yujun Wang, Ruo-Qian Wang, Carl Kamp, and Victor Wong. "Theoretical and experimental analysis of ash accumulation and mobility in ceramic exhaust particulate filters and potential for improved ash management." *SAE International Journal of Fuels and Lubricants* 7, no. 2014-01-1517 (2014): 511-524.
21. Lambert, Christine K., Mira Bumbaroska, Douglas Dobson, Jon Hangas, James Pakko, and Paul Tennison. "Analysis of High Mileage Gasoline Exhaust Particle Filters." *SAE International Journal of Engines* 9, no. 2016-01-0941 (2016): 1296-1304.
22. Bernardoff, Richard, Benjamin Hennebert, Thierry Delvigne, Olivier Courtois, and Philippe China. *A Study of Ash Accumulation in the After-treatment System of a Gasoline Direct Injection Engine Equipped with a Gasoline Particulate Filter*. No. 2017-01-0879. SAE Technical Paper, 2017.
23. Rubino, Lauretta, Dominic Thier, Torsten Schumann, Stefan Guettler, and Gerald Russ. *Fundamental Study of GPF Performance on Soot and Ash Accumulation over Artemis Urban and Motorway Cycles-Comparison of Engine Bench Results with GPF Durability Study on Road*. No. 2017-24-0127. SAE Technical Paper, 2017.
24. Lambert, Christine K., Timothy Chanko, Mark Jagner, Jon Hangas, Xin Liu, James Pakko, and Carl Justin Kamp. "Analysis of Ash in Low Mileage, Rapid Aged, and High Mileage Gasoline Exhaust Particle Filters." *SAE International Journal of Engines* 10, no. 2017-01-0930 (2017): 1595-1603.
25. Locker, Robert J., Natarajan Gunasekaran, and Constance Sawyer. *Diesel particulate filter test methods*. No. 2002-01-1009. SAE Technical Paper, 2002.
26. Arunachalam, Harikesh, Gabriele Pozzato, Mark A. Hoffman, and Simona Onori. "Modeling the thermal dynamics inside a ceria-coated Gasoline Particulate Filter." In *Control Technology and Applications (CCTA), 2017 IEEE Conference on*, pp. 99-105. IEEE, 2017.
27. Van Nieuwstadt, Michiel, and Joseph Ulrey. *Control Strategies for Gasoline Particulate Filters*. No. 2017-01-0931. SAE Technical Paper, 2017.
28. Lapuerta, Magín, Fermín Oliva, and Simón Martínez-Martínez. "Modeling of the soot accumulation in DPF under typical vehicle operating conditions." *SAE International Journal of Fuels and Lubricants* 3, no. 2010-01-2097 (2010): 532-542.
29. Rose, Dominik, and Thorsten Boger. *Different approaches to soot estimation as key requirement for DPF applications*. No. 2009-01-1262. SAE Technical Paper, 2009.
30. Boger, Thorsten, Dominik Rose, Per Nicolin, N. Gunasekaran, and Thomas Glasson. "Oxidation of soot (Printex® U) in particulate filters operated on gasoline engines." *Emission Control Science and Technology* 1, no. 1 (2015): 49-63.